SCHO-Optimized Fractional-Order Control Strategy for Enhanced Alternator Voltage Stability

Elouahab Bouguenna, Samir Ladaci, Bilal Taghezouit, Amine Berouaken, and Walid Merrouche

Abstract− This paper proposes a novel metaheuristic optimization framework grounded in the mathematical properties of hyperbolic trigonometric functions, introducing the Sinh–Cosh Optimizer (SCHO) as a bio-inspired algorithm that leverages the inherent gradient-like dynamics of sinh and cosh operators to achieve a principled and adaptive equilibrium between global exploration and local exploitation across complex search landscapes. The proposed framework is applied to tune an incommensurate Fractional-Order PID (FOPID) controller for Automatic Voltage Regulator (AVR) systems, where nonlinear dynamics and parametric uncertainties pose critical control challenges. The incommensurate non-integer differintegral structure extends the controller's degrees of freedom, enhancing its capacity to handle memory-dependent system behavior. Comparative simulations against conventional PID and standard FOPID benchmarks demonstrate a 32.115% overshoot reduction and a 33.335% ITSE improvement, with sustained robustness under load disturbances and parametric perturbations. The SCHO–FOPID strategy offers a scalable and mathematically rigorous intelligent control solution for uncertain nonlinear power systems, with direct applicability to smart grid and renewable energy contexts.

***Keywords*− sinh-cosh optimizer, fractional calculus, alternator voltage stability, robustness.**

I. Introduction

In modern power generation infrastructures, synchronous generators constitute the backbone of energy conversion from renewable sources to regulated electrical output. Nevertheless, terminal voltage deviations — induced by abrupt load transitions, mechanical torque oscillations, and electromagnetic disturbances — pose severe threats to the integrity of voltage-sensitive loads, including microprocessor-based systems and communication networks, where even marginal excursions can trigger irreversible failures [1], [2]. Automatic voltage regulators (AVRs) are therefore integrated into synchronous generator units as closed-loop excitation control mechanisms, continuously adjusting field current to confine output voltage within prescribed operational bounds.

Classical AVR implementations have long relied on proportional–integral–derivative (PID) controllers; however, the inherent rigidity of their integer-order structure renders them inadequate in the presence of system nonlinearities, unmodeled dynamics, and time-varying parametric uncertainties. Fractional calculus — which generalizes the order of differentiation and integration to the continuum of real numbers — has emerged as a mathematically rich and practically powerful paradigm for advanced control synthesis. Fractional-order PID (FOPID) controllers augment the classical three-parameter structure with two additional degrees of freedom, namely the integral order λ and the derivative order μ, yielding superior transient shaping, tighter reference tracking, and markedly improved disturbance rejection relative to their integer-order counterparts [3], [4]. From an analytical perspective, optimal FOPID parameterization necessitates resolving ill-conditioned fractional differential systems — a class of problems intrinsically amenable to population-based stochastic search [5]. Accordingly, metaheuristic optimization has established itself as the dominant paradigm for non-integer controller tuning, with representative contributions spanning chaos-augmented atom search strategies [6] and various hybrid swarm-based architectures [7]–[11] demonstrating consistent gains in closed-loop convergence and error minimization. Crucially, the No Free Lunch theorems (NFLTs) [12]–[15] formally establish that no optimizer holds universal dominance across arbitrary problem landscapes, thereby sustaining the imperative for algorithm diversity and continued methodological innovation. Preserving signal smoothness, solution correctness, and scalable performance under unmodeled dynamic conditions nonetheless remains an active and unresolved challenge.

Motivated by these considerations, this work investigates the Sinh–Cosh Optimizer (SCHO) [16], a recently introduced metaheuristic whose search mechanics are governed by the complementary analytical properties of hyperbolic trigonometric functions: the cosh component drives broad global exploration across the feasible space, while the sinh component orchestrates fine-grained local exploitation, collectively yielding a self-regulating and well-balanced optimization dynamic. Within the AVR control problem, SCHO is leveraged to identify the optimal parameter set of an incommensurate FOPID controller, targeting stable closed-loop behavior, accelerated convergence, and minimized steady-state tracking error under realistic disturbance and uncertainty scenarios.

The principal contributions of this study are threefold: **(i)** establishing the aptitude of SCHO for high-dimensional fractional-order tuning problems; **(ii)** formulating a stability-informed, constraint-aware optimization framework for

Manuscript received June 24, 2026; accepted July 2, 2026.

Elouahab Bouguenna and Samir Ladaci are with the Ecole Nationale Polytechnique, Algiers, ALGERIA. Bilal Taghezouit, Amine Berouaken, and Walid Merrouche are with CDER, Algeria.

Digital Object Identifier (DOI): 10.53907/enpesj.v6i1.393

FOPID synthesis; and **(iii)** demonstrating quantifiable dynamic performance gains under structured AVR parametric variations.

II. MATHEMATICAL MODEL OF AVR

An AVR constitutes a closed-loop excitation control architecture whose fundamental objective is to maintain the generator terminal voltage at a prescribed setpoint, irrespective of load fluctuations and varying operating conditions. By continuously confining the output voltage within allowable bounds, the AVR safeguards the reliability, power quality, and dynamic stability of the electrical supply delivered to downstream loads [17]. A representative configuration of an AVR-integrated power generation unit is illustrated in Fig. 1.

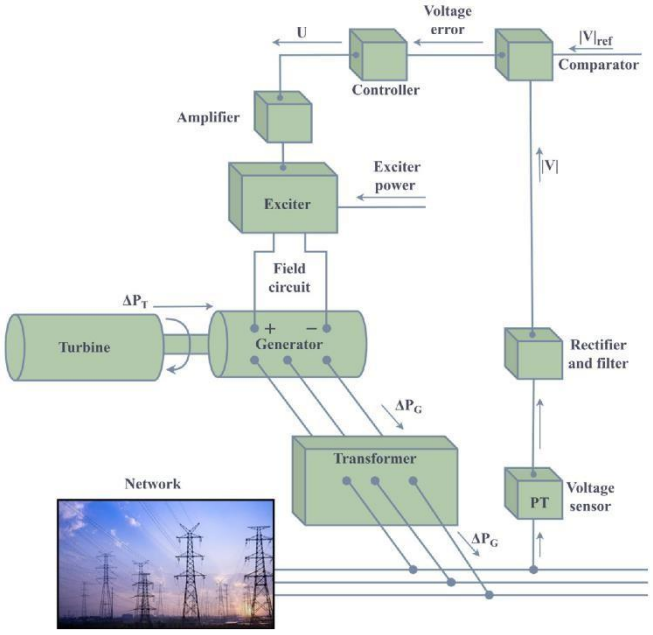

Fig. 1: Block diagram representation of the AVR loop.

In its basic operating principle, the AVR acquires a measurement of the terminal voltage, evaluates its deviation from a reference command, and processes the resulting error through an amplification stage to synthesize the appropriate control action. The generated signal is subsequently forwarded to the excitation subsystem, which modulates the generator field current and, consequently, the air-gap magnetic flux, steering the output voltage toward the target setpoint.

The detailed closed-loop structure of the regulated AVR system is depicted in Fig. 2, in which the synchronous generator acts as the primary controlled plant. A dedicated voltage transducer continuously acquires the output voltage and feeds it back to the summation node, where it is contrasted against the reference command. The resulting error signal quantifies the instantaneous discrepancy between the measured terminal voltage and its desired value. The controller interprets this error to compute the corrective excitation input in accordance with the governing control law, which acts upon the field current to drive the terminal voltage into convergence with the reference trajectory.

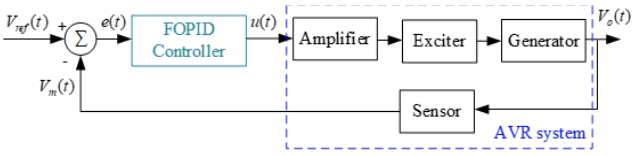

Fig. 2: Block diagram of a closed-loop AVR with feedback regulation.

Within this feedback architecture, the control design objectives transcend simple steady-state regulation. They encompass closed-loop stability preservation, robustness against parametric uncertainties and unmodeled system dynamics, bounded and smooth control effort, and minimization of residual tracking error. For analytical tractability, the voltage dynamics of an AVR-equipped synchronous generator are commonly represented by a first-order transfer function approximation [18]. Despite its simplicity, this reduced-order model adequately captures the dominant input–output voltage response characteristics and provides a practical and well-established foundation for controller synthesis and closed-loop stability assessment.

For reference, Table I compiles the transfer function models most widely adopted in the AVR literature, along with their associated parameter ranges, serving as a unified modeling basis for the comparative analysis conducted throughout this study.

Table. I

OPERATING LIMITS OF AVR SYSTEM PARAMETERS

Components	Transfer function	Gain	Time Constants (s)
Amplifier	$H_A(s)=\frac{G_a}{1+s\tau_a}$	$10 \le G_a \le 400$	$0.02 \le \tau_a \le 0.1$
Exciter	$H_E(s)=\frac{G_e}{1+s\tau_e}$	$1 \le G_e \le 10$	$0.4 \le \tau_e \le 1$
Generator	$H_G(s)=\frac{G_g}{1+s\tau_g}$	$0.7 \le G_g \le 1$	$1 \le \tau_g \le 2$
Sensor	$H_S(s)=\frac{G_s}{1+s\tau}$	$1 \le G_s \le 2$	$0.001 \le \tau_s \le 0.06$

In which τ_a, τ_e, τ_g, and τ_s represent the amplifier, exciter, generator, and sensor time constants, respectively, while G_a, G_e, G_g, and G_s represent their associated gains. The parameter values listed below, constituting the primary basis of this study, have been selected for AVR system evaluation [19].

$$G_a = 10,\ G_e = 1,\ G_g = 1,\ G_s = 1,$$
$$\tau_a = 0.1\ \text{s},\ \tau_e = 0.4\ \text{s},\ \tau_g = 1\ \text{s},\ \tau_s = 0.01\ \text{s},$$

It is worth noting that the generator gain G_g does not remain fixed but exhibits a load-dependent variability intrinsic to the operating regime of the synchronous machine. Specifically, G_g spans a range from approximately 0.7 under no-load conditions to unity at rated loading [20], a characteristic that directly reflects the nonlinear nature and parametric sensitivity of the generator subsystem. Grounding the analysis in the linearized transfer function representations of the individual AVR components, the aggregate closed-loop transfer function governing the overall AVR system dynamics is expressed as:

$$H(s) = \frac{0.1s + 10}{0.0004s^4 + 0.0454s^3 + 0.555s^2 + 1.51s + 11} \quad (1)$$

For $G_g = 1$, the closed-loop feedback system exhibits the following pole locations:

$s_{1,2} = -0.5198 \pm 4.6642i,\ s_3 = -12.4891,\ s_4 = -99.9711$

For $G_g = 0.7$, the closed-loop feedback system exhibits the following pole locations:

$s_{1,2} = -0.7959 \pm 4.017i, s_3 = -11.9284, s_4 = -99.9798$

A standard tool for assessing closed-loop stability is root locus analysis, which traces the migration of system poles across the complex plane as the feedback gain is varied. Consistent with classical control theory, a system is deemed asymptotically stable if and only if all characteristic poles are confined to the open left-half of the s-plane. The computed pole locations satisfy this condition, thereby validating the asymptotic stability of the AVR closed-loop system under the proposed control architecture.

III. BASICS OF FRACTIONAL CALCULUS

Fractional-order calculus extends the classical integer-order framework of differentiation and integration to the broader domain of arbitrary real — and even complex — orders. The conceptual origins of non-integer derivatives trace back to Leibniz in 1695, with subsequent rigorous mathematical foundations established through the independent contributions of Liouville, Grünwald, Letnikov, and Riemann. The unified differintegral operator ${}_a\mathcal{D}_t^{\alpha}$, where a and t denote the lower and upper bounds of the operation respectively, and $\alpha \in R$ governs the order of differentiation or integration, serves as the cornerstone of this generalized calculus. Beyond mere mathematical abstraction, this operator provides a versatile and physically meaningful tool for characterizing the memory effects and hereditary dynamics that pervade a wide class of real-world systems. Its formal definition is given by:

$$ {}_a\mathcal{D}^{\alpha} = \begin{cases} d^{\alpha}/dt^{\alpha} & \text{for } \Re(\alpha) > 0 \\ \int_a^t (d\tau)^{-\alpha} & \text{for } \Re(\alpha) < 0 \\ 1 & \text{for } \Re(\alpha) = 0 \end{cases} \tag{2} $$

Among the several established definitions of fractional-order derivatives, the Caputo formulation stands as the most prevalent and practically favored in engineering applications, owing to its compatibility with classical integer-order initial conditions. For a sufficiently smooth function $f(t) \in C^{n+1}\left([0,+\infty), R\right)$ is given by [2]:

$$ {}^{C}\mathcal{D}^{\alpha} f(t) = \frac{1}{\Gamma(n-\alpha)} \int_0^t \frac{f^{(n)}(\xi)}{(t-\xi)^{\alpha-n+1}} d_{\xi} \tag{3} $$

where $\Gamma(x)$ denotes the Gamma function, defined as:

$$ \Gamma(x) = \int_0^{\infty} y^{x-1} e^{-y} dy \tag{4} $$

Under the assumption of zero initial conditions — a standard premise in linear control analysis — the Laplace transform provides an effective and tractable tool for characterizing fractional-order systems in the frequency domain. Accordingly, the Laplace-domain representation of the Caputo fractional derivative of order $\alpha \in \mathbb{R}^+$ reduces to:

$$ \mathcal{L}\left\{\mathcal{D}^{\alpha} f(t), s\right\} = s^{\alpha} F(s) \tag{5} $$

This formulation yields transfer functions parameterized by non-integer powers of the complex variable ss s, reflecting the infinite-dimensional nature of fractional-order operators. Since an exact realization of such operators would, in principle, demand an unbounded cascade of poles and zeros, practical deployment — whether in numerical simulation environments or physical hardware implementations — necessitates the use of finite-order rational approximations. These reduced representations are constructed to faithfully replicate the essential frequency-domain behavior of the original fractional operator while maintaining computational tractability. A representative and widely referenced approach is the recursive pole-zero distribution scheme introduced by Charef [21], which achieves accurate rational approximation of fractional powers of ss s over a prescribed frequency band. This methodology underpins the construction of rational transfer function approximations of fractional operators, expressed in the general form:

$$ G(s) = s^{\alpha}, \quad \alpha \in R^{+} \tag{6} $$

Into a rational function represented as a ratio of polynomials expressed in a factorized form:

$$ \hat{G}(s) = \frac{\sum_{i=0}^{n-1} (1 + s/z_i)}{\sum_{i=0}^{n} (1 + s/p_i)} \tag{7} $$

where the coefficients are determined such that the approximation yields a maximum error of y dB relative to the baseline frequency-domain magnitude response.

By establishing:

$$ a = 10^{y/10(1-\alpha)},\ b = 10^{y/10\alpha} $$

The locations of zeros and poles inherent in the resulting rational approximation are determined using the following analytical expressions:

$$ z_0 = \omega_c \sqrt{b},\ p_0 = a z_0,\ z_i = (ab)^i z_0,\ p_i = (ab)^i a z_0 $$

The total number of zeros and poles is directly linked to the specified bandwidth and the admissible approximation error, as defined by the following relation:

$$ N = \text{integer}\left\lfloor \frac{\lceil \log(\omega_{\max} / z_0) \rceil}{\log(ab)} + 1 \right\rfloor $$

IV. FRACTIONAL-ORDER CONTROLLER

The concept of employing fractional-order controllers for dynamic systems was pioneered by Oustaloup, who introduced the CRONE control strategy [22]. The non integer PID control represents an extended form of the conventional PID architecture, extending its capability through non-integer differentiation and integration orders. This enhanced flexibility allows for finer tuning of closed-loop performance, improved robustness against uncertainties, and superior handling of complex system dynamics. The FOPID controller is mathematically represented by the following transfer function:

$$ G_c(s) = \frac{U(s)}{E(s)} = K_p + K_i s^{-\lambda} + K_d s^{\mu},\ \ \lambda, \mu > 0 \tag{8} $$

The time domain equation for such controller has the form:

$$ u(t) = K_p e(t) + K_i \mathcal{D}^{-\lambda} e(t) + K_d \mathcal{D}^{\mu} e(t) \tag{9} $$

where $u(t)$ denotes the control input and $e(t)$ represents the associated error signal.

Specifically, the FOPID controller encompasses several classical structures as special cases. The parameter pairs $(\lambda, \mu) = (1,1)$, $(0,1)$, $(1,0)$, and $(0,0)$ corresponds respectively

to the conventional PID, PD, PI, and proportional controllers. As illustrated in Fig.3.

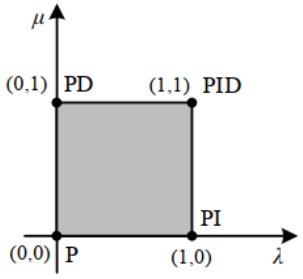

Fig. 3: Visualization of the FOPID controller structure and operation.

The architecture of the FOPID control law is illustrated in Fig. 4.

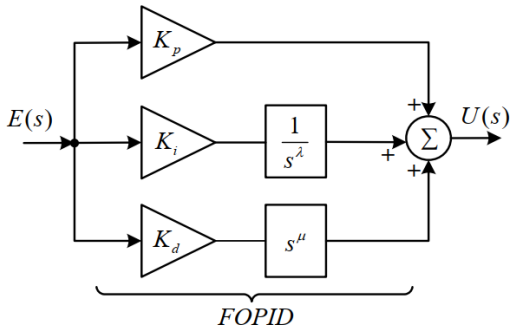

Fig. 4: FOPID controller structure.

V. SINH-COSH ALGORITHM

A. Initialisation case

As with most metaheuristic optimization methods, the SCHO algorithm initializes by generating a population of candidate solutions at random. This population, expressed in (10), is then iteratively updated through the search process, and the best-performing candidate at the end of the iterations is taken as an approximation of the global optimum [16].

$$X = \begin{bmatrix} x_{1,1} & \cdots & x_{1,j} & x_{1,\dim-1} & x_{1,\dim} \\ x_{2,1} & \cdots & x_{2,j} & \cdots & x_{2,\dim} \\ \cdots & \cdots & x_{i,j} & \cdots & \cdots \\ \vdots & \vdots & \vdots & \vdots & \vdots \\ x_{N-1,1} & \cdots & x_{N-1,j} & \cdots & x_{N-1,\dim} \\ x_{N,1} & \cdots & x_{N,j} & x_{N,\dim-1} & x_{N,\dim} \end{bmatrix} \quad (10)$$

In this context X denotes the population of candidate solutions generated by (11), where N specifies the population size, $x_{i,j}$ corresponds to the j^{th} element of the i^{th} solution vector, and *dim* represents the dimensionality of the search space.

$$X = rand(N, \dim) \times (ub - lb) + lb \quad (11)$$

where *rand* represents a random variable uniformly distributed across the interval [0,1], whereas *ub* and *lb* correspond to the upper and lower bounds of the decision variables, respectively.

B. Exploration case

The exploration stage is governed by a position–updating mechanism, mathematically expressed through the following relation:

$$X_{(i,j)}^{t+1} = \begin{cases} X_{best}^{(j)} + r_1 \times W_1 \times X_{(i,j)}^{t}, & r_2 > 0.5 \\ X_{best}^{(j)} - r_1 \times W_1 \times X_{(i,j)}^{t}, & r_2 < 0.5 \end{cases} \quad (12)$$

In this formulation, t represents the current iteration index, while $X_{(i,j)}^{t+1}$ and $X_{(i,j)}^{t}$ denote the j^{th} element of the i^{th} solution vector at the next and current iterations, respectively.

W_1 denotes the weight coefficient defined as:

$$W_1 = r_3 \times a_1 \times (\cosh r_4 + u \times \sinh r_4 - 1) \quad (13)$$

where r_1 – r_4 are random numbers between 0 and 1. The parameter u is a sensitivity coefficient that regulates the exploration accuracy in the first phase and is fixed at 0.388.

$$a_1 = 3 \times \left(-1.3 \times \frac{t}{Max\_iteration} + m \right) \quad (14)$$

Here m is a sensitivity coefficient that governs the exploration accuracy and is set to 0.45 based on experimental results in [16], and t is a coefficient that defines the switching point between the two phases and is fixed at 3.6, as reported in [16].

C. Exploration case

In swarm intelligence (SI) optimization, the exploitation mechanism remains active during the entire evolutionary process. To reinforce search efficiency, this mechanism is structured into two complementary phases, both executed across all iterations. In the first phase, the search is concentrated in the local neighborhood of X, and the corresponding exploitation update is formulated as [16]:

$$X_{(i,j)}^{t+1} = \begin{cases} X_{best}^{(j)} + r_5 \times W_2 \times X_{(i,j)}^{t}, & r_6 > 0.5 \\ X_{best}^{(j)} - r_5 \times W_2 \times X_{(i,j)}^{t}, & r_6 < 0.5 \end{cases} \quad (15)$$

where W_2 is the weight coefficient given by [16]:

$$W_2 = r_7 \times a_1 \times (\cosh r_8 + u \times \sinh r_8) \quad (16)$$

and r_5 to r_8 are random numbers between 0 and 1. The parameter u retains the same value as in the first exploration phase, being fixed at 0.388.

VI. OPTIMIZATION METHODOLOGY

In the design of controllers, there are several performance criterions. The often-used criterions are the integral of absolute error (IAE) and the integral of squared error (ISE). In this paper, the IAE, expressed in (17), is applied as the objective function due to its strong relevance in voltage regulation problems, particularly for minimizing steady-state tracking error and transient deviations. At each iteration, the voltage error signal given by (18) is utilized to compute the index, while the SCHO algorithm iteratively searches for the optimal set of controller parameters.

$$J = IAE = \int_0^t |e(t)| dt \quad (17)$$

$$e(t) = V_{ref}(t) - V_{out}(t) \quad (18)$$

The parameterization of the FOPID controller consists of five degrees of freedom (5-DoF), specifically three gain terms and two fractional orders, each restricted to specific ranges and investigated within the defined optimization space.

$$K_p^{\min} \le K_p \le K_p^{\max}, \quad K_i^{\min} \le K_i \le K_i^{\max}, \quad K_d^{\min} \le K_d \le K_d^{\max}$$

$$\alpha^{\min} \le \alpha \le \alpha^{\max}, \quad \beta^{\min} \le \beta \le \beta^{\max}$$

These limits represent the upper and lower bounds (*ub* and *lb*) defined in (11). Based on prior literature and practical design considerations, the feasible parameters ranges adopted in this study are:

$$0 \le K_p \le 3, \quad 0 \le K_i \le 3, \quad 0 \le K_d \le 3, \quad 0 \le \alpha \le 2, \quad 0 \le \beta \le 2$$

It is worth highlighting that incorporating a FOPID controller into the feedback loop may, for certain parameter configurations, jeopardize closed-loop stability. To address this challenge, a constraint-aware optimization strategy is employed in this work. Each candidate solution—representing a unique combination of FOPID parameters—is thoroughly assessed to ensure stability guarantee of the system, with poles located strictly in the left-half *s*-plane and trajectories converging asymptotically. Any candidate leading to instability is systematically discarded, regardless of its fitness value.

Fig. 5 illustrates the optimization framework employed for tuning the FOPID controller parameters.

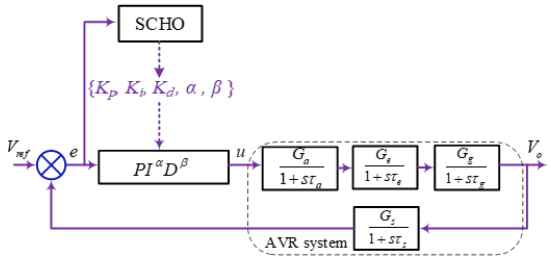

Fig. 5: SCHO-based FOPID optimization framework

VII. SIMULATION RESULTS

This section evaluates the effectiveness of the proposed SCHO-optimized FOPID controller for AVR regulation. The closed-loop performance achieved with the SCHO-based FOPID is systematically compared against conventional controllers, including the PI and standard FOPID schemes and other algorithms-based controllers. As an initial step, and based on the transfer function given in (1), the AVR system is examined in its basic feedback configuration without any external controller. The corresponding response, shown in Fig. 6, reveals oscillatory and weakly damped dynamics, with the feedback loop alone unable to suppress instability. Consequently, the control input *u* fails to provide adequate stabilization, leading to persistent oscillations and divergence from the reference signal.

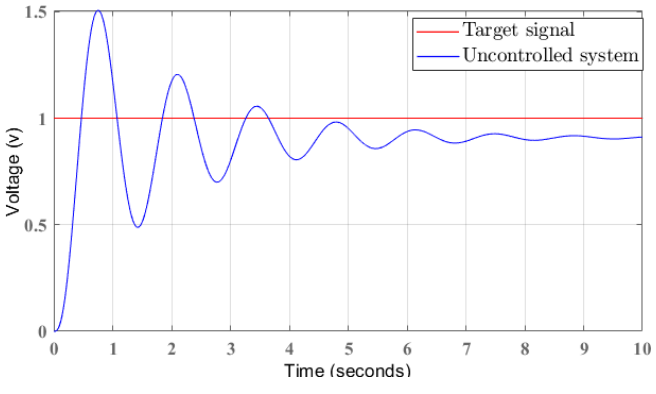

Fig. 6: SCHO-based FOPID optimization framework

Based on the Ziegler–Nichols tuning method, the FOPID controller parameters are initially determined. The fractional orders are approximated using an 8th-order filter ($N = 8$) with a maximum magnitude error of 1 dB ($y = 1$ dB) over the frequency range $\omega \in \lceil \lfloor 10^{-3}, 10^{3} \rceil \rfloor$ rad/s. The SCHO algorithm is then employed to optimally refine the FOPID parameters. In SCHO, the population size is set to 30 and the number of iterations to 50, ensuring an effective balance between exploration and exploitation. The optimization process is repeated 20 times to ensure thorough evaluation, and the best solution among the 20 runs is selected as the controller parameters for the simulations.

A comparative assessment of the AVR terminal voltage response under different control strategies is illustrated in Fig. 7. The performance of the proposed SCHO-optimized FOPID controller is benchmarked against PI and standard FOPID controllers.

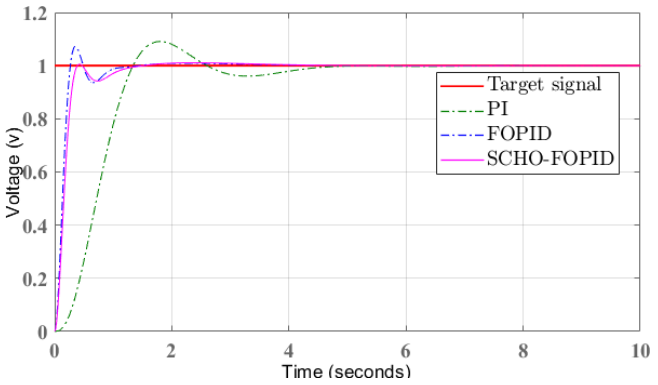

Fig. 7: AVR step response: PI vs. FOPID vs. SCHO-FOPID.

From the closed-loop responses, several critical observations can be drawn. First, the PI controller, while able to regulate the terminal voltage, exhibits a relatively sluggish transient response, marked by a slower rise time, larger overshoot, and extended settling period. These characteristics suggest limited effectiveness in applications requiring rapid stabilization of generator terminal voltage under sudden load disturbances. The standard FOPID controller provides a noticeable improvement by leveraging fractional calculus to enhance the system's memory effect and flexibility in feedback shaping. This results in faster convergence compared to PI control and reduced oscillations. However, the transient performance still suffers from noticeable overshoot and longer settling time, indicating that stability margins remain suboptimal. By contrast, the SCHO-FOPID controller delivers a superior dynamic profile. The closed loop response exhibits: minimal overshoot, rapid rise time and significantly shorter settling time and negligible steady-state error. The SCHO-FOPID reduces overshoot by 86.22% compared with the FOPID controller and by 88.35% compared with the PI controller. Additionally, The SCHO-FOPID reduces settling time by 77.38% compared with the PI controller and by 1.76% compared with the FOPID. The optimal parameter set of the SCHO-FOPID is reported in Table II, while Table III presents a comprehensive comparison of the transient response indices obtained for all controllers.

Table. II

SIMULATION PARAMETERS SETTING USING SCHO

K_p	K_i	K_d	α	β
0.9382	0.6371	0.3742	1.2115	0.9045

Table. III

PERFORMANCE INDICES COMPARISON

Parameters	**Controller**		
	SCHO-FOPID	**FOPID**	**PI**
K_p	0.9382	0.8252	0.1877
K_i	0.6371	1.6051	0.1388
K_d	0.3742	2.1590	-
α	1.2115	0.8541	-
β	0.9045	0.9357	-
Settling time t_s (s)	**1.1347**	1.1550	5.0087
Rise time t_r (s)	0.3826	**0.2436**	1.3391
Overshoot (%)	**1.2400**	9.0000	10. 6300

Another comparative analysis is carried out with respect to the state-of-the-art optimization methods, namely ABC and AHA, while uniform constraints were applied across all algorithms: a population size of 50 candidate solution set, a maximum of 100 iterations, and 5 search variables. Each algorithm was run independently 10 times to account for stochastic variability. As shown in Fig. 8, the SCHO-FOPID approach exhibits superior voltage stability within the AVR system, achieving the lowest overshoot and fastest settling time, while ABC-FOPID yields the shortest rise time. Furthermore, SCHO-FOPID provides a smoother transient response with minimal oscillations, demonstrating strong robustness against unmodeled dynamics and load disturbances. These results confirm its improved closed-loop stability and dynamic performance, ensuring higher reliability for AVR applications in renewable energy systems. The key reference-tracking results for all optimization-based FOPID control are listed in Table IV.

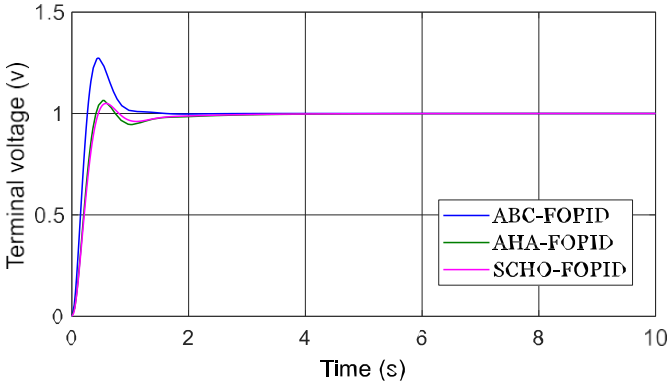

Fig. 8: AVR step response comparison using different FOPID tuning algorithms.

. **Table. IV**

COMPARISON OF DIFFERENT ALGORITHMS

Time response spesifcations	**Controller**		
	SCHO-FOPID	*AHA-FOPID*	*ABC-FOPID*
Settling time t_s (sec)	**1.4750**	1.7680	1.8010
Rise time t_r (sec)	0.4376	0.4096	**0.2647**
Overshoot (%)	**6.0300**	6.4400	27.3100

A central requirement of the FOPID controller design is to guarantee closed-loop stability and deliver a well-shaped step response, particularly in the face of abrupt parametric excursions. To this end, a systematic robustness assessment of the SCHO-optimized FOPID-controlled AVR system has been carried out, wherein the plant time constants are individually perturbed across a symmetric range of ±50% around their nominal values in discrete increments of 25%. The resulting closed-loop responses under the proposed control strategy are depicted in Fig. 9. The SCHO-tuned FOPID architecture consistently demonstrates enhanced transient characteristics and sustained resilience against model uncertainty throughout the entire perturbation range. Inspection of the output trajectories reveals that the system response remains confined within a remarkably narrow deviation band, attesting to the exceptional parametric robustness conferred by the proposed controller. These findings collectively confirm the capacity of the SCHO–FOPID scheme to preserve closed-loop stability and regulation quality across the full spectrum of examined parameter variations.

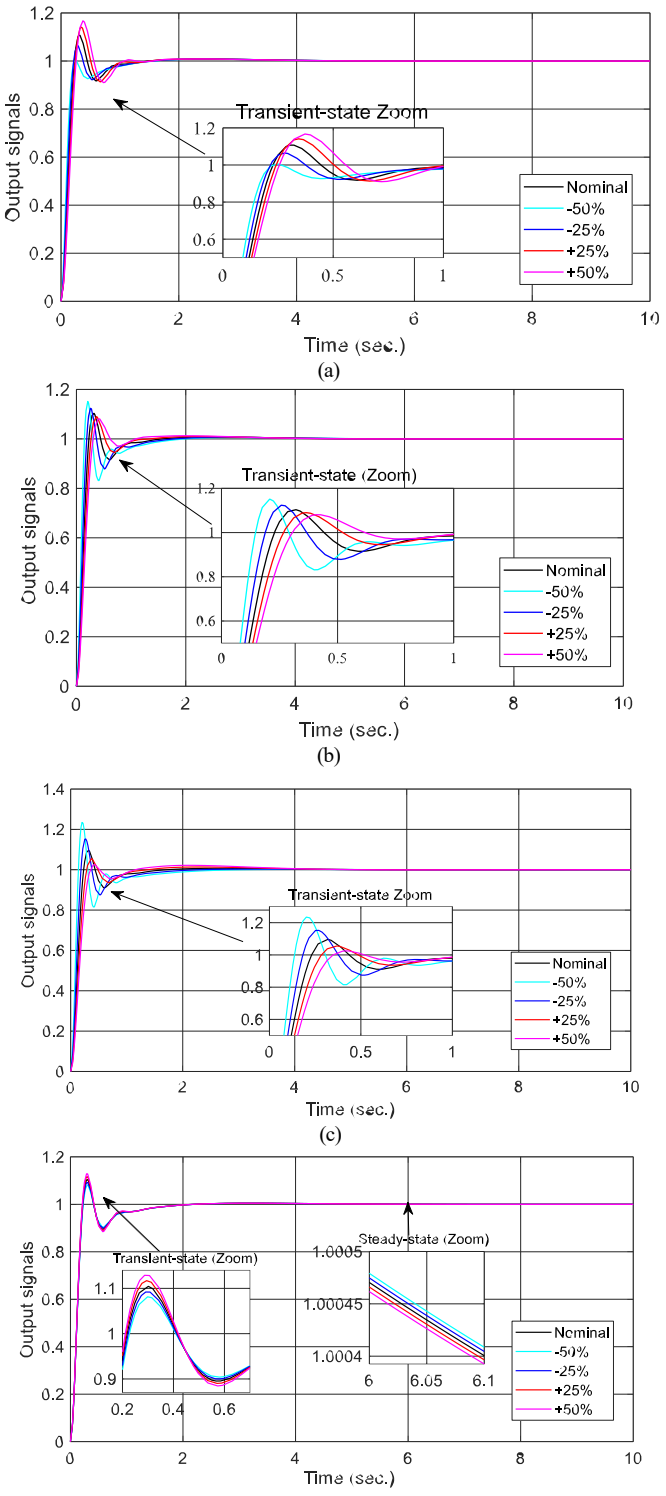

Fig. 9: Robustness analysis of the SCHO-FOPID-controlled AVR under sudden variations in time constant parameters for (a) T_a, (b) T_e, (c) T_g, (d) T_s.

VIII. CONCLUSION

This study presented a systematic and computationally intelligent framework for the optimal synthesis of a Fractional-Order PID (FOPID) controller applied to the Automatic Voltage Regulator (AVR) problem, a critical benchmark for nonlinear power system control under parametric uncertainty. The Sinh–Cosh Optimizer (SCHO), a novel metaheuristic grounded in the complementary analytical dynamics of hyperbolic trigonometric functions, was employed to simultaneously and optimally calibrate the five degrees of freedom (5-DoF) of the FOPID structure, encompassing the proportional, integral, and derivative gains alongside the non-integer integration and differentiation orders.

The synergistic integration of fractional calculus with computational intelligence endows the proposed SCHO–FOPID scheme with a markedly expanded control authority relative to classical integer-order architectures. This expanded parameterization enables the controller to capture memory-dependent and hereditary system dynamics, resulting in superior closed-loop accuracy, enhanced transient shaping, and robust steady-state regulation under diverse operating conditions.

Simulation results unambiguously validated the effectiveness of the proposed strategy in compensating for system nonlinearities, unmodeled dynamics, and abrupt load disturbances. Rigorous comparative benchmarking against classical PID, standard FOPID, and state-of-the-art metaheuristic-tuned controllers (including those based on the Artificial Bee Colony (ABC) and Artificial Hummingbird Algorithm (AHA) optimizers) confirmed the quantitative superiority of the SCHO–FOPID scheme. Specifically, the proposed controller achieved a 19.86% reduction in settling time and a 6.80% decrease in overshoot relative to the AHA-tuned FOPID benchmark, alongside a significant improvement in the ITSE performance index, collectively reflecting accelerated convergence and tighter reference tracking.

Robustness evaluations conducted under structured parametric perturbations — spanning ±50% variations in the AVR plant time constants — further demonstrated the controller's capacity to maintain stable and well-regulated closed-loop behavior across a wide uncertainty envelope, without significant degradation in dynamic performance. These results underscore the resilience of the fractional-order control paradigm when coupled with a well-balanced optimization algorithm.

From a broader perspective, this work reinforces the growing relevance of fractional-order intelligent control in addressing the increasingly complex demands of modern power systems, particularly in renewable energy integration and smart grid contexts, where nonlinearity, intermittency, and parameter variability are inherent operational realities.

Future research directions may encompass the extension of the SCHO–FOPID framework to multi-machine power system configurations, its adaptation for real-time embedded implementation on hardware platforms, and the incorporation of adaptive or self-tuning mechanisms to address time-varying and nonstationary operating environments. The investigation of incommensurate fractional structures and their interaction with advanced stability certification tools also represents a promising avenue for subsequent contributions.

REFERENCES

[1] W. M. Alghamdi and M. O. Alassafi, “Effective Alternator Voltage Control Based on Computational Intelligence Using Dream Optimizer,” 2026.

[2] E. Bouguenna, S. Ladaci, B. Lekouaghet, W. Merrouche, and M. Benghanem, “Fractional Order PID Controller Design for an AVR System Using the Artificial Hummingbird Optimizer Algorithm,” *Int. J. Robust Nonlinear Control*, pp. 1–25, 2025, doi: 10.1002/rnc.7894.

[3] I. Podlubny, “Fractional-order systems and PIλDμ-controllers,” *IEEE Trans. Autom. Control. 1999,* vol. 44, no. 1, pp. 208–214.

[4] S. Ladaci, J. J. Loiseau, and A. Charef, “Fractional order adaptive high-gain controllers for a class of linear systems,” *Commun. Nonlinear Sci. Numer. Simul.*, vol. 13, no. 4, pp. 707–714, 2008, doi: 10.1016/j.cnsns.2006.06.009.

[5] E. Bouguenna, S. Ladaci, and W. Merrouche, “Stability and Performance Enhancement of a Step-Down Converter in Photovoltaic Systems Using an Optimization Algorithm-Based Fractional PIλDδ Controller,” pp. 170–178, 2025, doi: 10.1007/978-3-031-80301-7_19.

[6] B. Hekimoğlu, “Optimal Tuning of Fractional Order PID Controller for DC Motor Speed Control via Chaotic Atom Search Optimization Algorithm,” *IEEE Access*, vol. 7, pp. 38100–38114, 2019, doi: 10.1109/ACCESS.2019.2905961.

[7] S. Ekinci, C. Turkeri, I. Gokalp, Y. Li, and D. Li, “High-performance temperature regulation of nonlinear CSTRs via a hybrid stellar oscillation optimizer and differential evolution-based PID-F control,” *Sci. Rep.*, vol. 16, no. 1, 2026, doi: 10.1038/s41598-026-38354-5.

[8] W. Merrouche, B. Lekouaghet, and E. Bouguenna, “Adolescent Identity Search Algorithm (AISA) for Li-ion Battery Electrical Model Optimization,” *Int. J. Artif. Intell. Tools Appl.*, vol. 2, no. 1, 2024.

[9] A. M. Mosaad, M. A. Attia, N. M. Elbehairy, M. Alruwaili, A. Yousef, and N. M. Hamed, “Enhancing AVR System Stability Using Non-Monopolize Optimization for PID and PIDA Controllers,” pp. 1–17, 2025.

[10] M. S. Ayas and E. Sahin, “FOPID controller with fractional filter for an automatic voltage regulator,” *Comput. Electr. Eng.*, vol. 90, no. April 2020, p. 106895, 2021, doi: 10.1016/j.compeleceng.2020.106895.

[11] Ö. Can, M. Ş. Ayas, and E. Çelik, “Frequency and voltage stability improvement in a two-area thermal power system using a novel controller and RIME optimizer,” *Comput. Electr. Eng.*, vol. 125, p. 110434, Jul. 2025, doi: 10.1016/j.compeleceng.2025.110434.

[12] W. Merrouche, B. Lekouaghet, I. A. E. Boughiout, E. Bouguenna, and M. Benghanem, “Fully Informed Search Algorithm for Estimating the Parameters of Li-Ion Battery Model under UDDS Drive Cycle Profile,” *Transp. Res. Procedia*, vol. 84, pp. 275–282, 2025, doi: 10.1016/j.trpro.2025.03.073.

[13] W. Merrouche, B. Lekouaghet, and E. Bouguenna, “Gaussian Quantum-behaved PSO strategy for Lithium Battery model optimization,” in *2023 International Symposium on Quantum Sciences: Applications and Challenges (QSAC2023)*, Algiers, 2023, p. 13.

[14] T. Joyce and J. M. Herrmann, “A Review of No Free Lunch Theorems, and Their Implications for Metaheuristic Optimisation,” 2018, pp. 27–51. doi: 10.1007/978-3-319-67669-2_2.

[15] E. Bouguenna, S. Ladaci, and B. Taghezouit, “Robust Optimal Fractional-Order PIλ-PDμ Cascade Control Using a PID- Inspired Search Algorithm for DC-DC Converters,” *IFAC Pap.*, vol. 59, no. 37, pp. 250–255, 2026, doi: 10.1016/j.ifacol.2026.01.043.

[16] J. Bai *et al.*, “A Sinh Cosh optimizer,” *Knowledge-Based Syst.*, vol. 282, no. September, p. 111081, 2023, doi: 10.1016/j.knosys.2023.111081.

[17] G. Singh, D. Kumar, P. Aryan, T. R. Chelliah, and G. L. Raja, “Robust and Unified Fractional Order AGC-AVR Scheme for Hydropower Plant,” *IEEE Trans. Ind. Appl.*, vol. PP, pp. 1–14, 2026, doi: 10.1109/TIA.2026.3675039.

[18] E. Bouguenna and S. Ladaci, “Hippopotamus Optimization Algorithm-Based Robust Tilt-FOID Control Design for Linear Time-Invariant Systems in Renewable Energy Applications,” *2025 Int. Conf. Artif. Intell. Embed. Syst. Renew. Energy*, pp. 1–6, 2025, doi: 10.1109/AIESRE67541.2025.11470220.

[19] E. Bouguenna, B. Lekouaghet, and M. Haddad, “Improved Fractional PIαDβ Controller for AVR System via a New Optimization Algorithm,” *2024 2nd Int. Conf. Electr. Eng. Autom. Control. ICEEAC 2024*, 2024, doi: 10.1109/ICEEAC61226.2024.10576215.

[20] S. Ekinci and B. Hekimoglu, “Improved Kidney-Inspired Algorithm Approach for Tuning of PID Controller in AVR System,” pp. 39935–39947, 2019.

[21] A. Charef, H. H. Sun, Y. Y. Tsao, and B. Onaral, “Fractal system as represented by singularity function,” *IEEE Trans. Automat. Contr.*, vol. 37, no. 9, pp. 1465–1470, 1992, doi: 10.1109/9.159595.

[22] A. Oustaloup, F. Levron, B. Mathieu, and F. M. Nanot, “Frequency-band complex noninteger differentiator: Characterization and synthesis,” *IEEE Trans. Circuits Syst. I Fundam. Theory Appl.*, vol. 47, no. 1, pp. 25–39, 2000, doi: 10.1109/81.817385.